**Atmospheric
Chemistry
and Physics**

Isotope effect in the formation of H_2 from H_2CO studied at the atmospheric simulation chamber SAPHIR

T. Röckmann[1]**, S. Walter**[1]**, B. Bohn**[2]**, R. Wegener**[2]**, H. Spahn**[2]**, T. Brauers**[2]**, R. Tillmann**[2]**, E. Schlosser**[2,*]**,
R. Koppmann**[3]**, and F. Rohrer**[2]

[1]Institute for Marine and Atmospheric research Utrecht, Utrecht University, Utrecht, The Netherlands
[2]Institut für Chemie und Dynamik der Geosphäre ICG-2, Forschungszentrum Jülich GmbH, Jülich, Germany
[3]Faculty of Mathematics and Natural Sciences, University of Wuppertal, Wuppertal, Germany
[*]now at: Institut für Meteorologie und Klimaforschung, Karlsruhe Institute of Technology, Karlsruhe, Germany

Abstract. Formaldehyde of known, near-natural isotopic composition was photolyzed in the SAPHIR atmosphere simulation chamber under ambient conditions. The isotopic composition of the product H_2 was used to determine the isotope effects in formaldehyde photolysis. The experiments are sensitive to the molecular photolysis channel, and the radical channel has only an indirect effect and cannot be effectively constrained. The molecular channel kinetic isotope effect KIE_{mol}, the ratio of photolysis frequencies $j(HCHO \rightarrow CO + H_2)/j(HCDO \rightarrow CO + HD)$ at surface pressure, is determined to be $KIE_{mol} = 1.63^{+0.038}_{-0.046}$. This is similar to the kinetic isotope effect for the total removal of HCHO from a recent relative rate experiment ($KIE_{tot} = 1.58 \pm 0.03$), which indicates that the KIEs in the molecular and radical photolysis channels at surface pressure (≈ 100 kPa) may not be as different as described previously in the literature.

1 Introduction

Molecular hydrogen (H_2) is the second most abundant reduced gas in the atmosphere after methane with a global average mixing ratio of roughly 500 ppb. Interest in its atmospheric cycle has strongly increased in the past years because of its potential future large-scale use as energy carrier. Since use of H_2 only produces H_2O, a future hydrogen economy is expected to ameliorate many of the present climate

and air quality related problems (Schultz et al., 2003). However, it is expected that unavoidable leaks in the production, storage, transport and use of H_2 would considerably increase the atmospheric content of H_2. Although H_2 is not a greenhouse gas, it affects the concentration of the greenhouse gas methane and many other species via a feedback from its removal reaction with the hydroxyl (OH) radical (Schultz et al., 2003). In the stratosphere, increased levels of H_2 will lead to higher levels of stratospheric water vapor, which will change the radiative budget of the stratosphere. Enhanced levels of stratospheric aerosol may also alter ozone chemistry, e.g., through enhanced N_2O_5 hydrolysis affecting the catalytic O_3 destruction cycles. In Polar Regions, enhanced water can lead to an increase in the occurrence of polar stratospheric clouds (PSC) in winter (Schultz et al., 2003; Tromp et al., 2003; Warwick et al., 2004; Feck et al., 2008). PSC play a key role in the halogen-catalyzed destruction of ozone (the ozone hole), and thus increased H_2 levels are expected to delay the recovery of the polar ozone hole.

H_2 has a peculiar latitudinal distribution in the atmosphere with higher mixing ratios in the Southern Hemisphere (SH) compared to the Northern Hemisphere (NH) (Steele et al., 1996; Novelli et al., 1999; Ehhalt and Rohrer, 2009). This is because the main H_2 removal process is deposition to soils, and there is much more soil surface in the NH. The second important removal process is oxidation by the OH radical. H_2 is produced mainly by three classes of processes: 1) combustion processes (fossil fuel burning and biomass burning) 2) photolysis of formaldehyde (HCHO), which is a relatively stable intermediate in the atmospheric oxidation chains of CH_4 and non-methane hydrocarbons (NMHC) and

3) biological processes in the soil or the ocean. The third group is likely of minor importance, but there are still large error bars on the quantitative estimates of all sources and sinks of H_2.

Isotope studies can yield valuable insight into the relative strengths of sources and sinks of atmospheric H_2. H_2 emitted from different sources usually carries a distinct isotope composition and the kinetic isotope effects in the two sinks differ strongly (Gerst and Quay, 2000, 2001; Rahn et al., 2003, 2002a, b; Rhee et al., 2004, 2005, 2008; Brenninkmeijer et al., 2003; Röckmann et al., 2003, 2010; Vollmer et al., 2010). In the case of hydrogen the isotope effects are particularly large due to the 100% relative mass difference between ^1H and ^2H (deuterium, in the following denoted D). The isotope ratio is measured as a ratio of the rare isotope D to the abundant isotope H and expressed as difference to the isotope ratio of Standard Mean Ocean Water (V-SMOW, $(D/H)_{VSMOW}=1.56\times10^{-4}$) given in per mil units ($\delta D=[(D/H)_{Sa}/(D/H)_{VSMOW}-1]$). The average isotopic composition of atmospheric H_2 is roughly +130‰. Emissions from the ocean and nitrogen fixation in soils are expected to have the lowest D content ($\delta D \sim -700$‰), due to the equilibrium fractionation between water and H_2 (Bottinga, 1968). δD values between -200 and -300‰ have been determined for H_2 from biomass and fossil fuel burning (Gerst and Quay, 2001; Rahn et al., 2002b; Röckmann et al., 2010; Vollmer et al., 2010). Atmospheric oxidation processes must have an enriched isotope signature to balance the isotope budget, as first postulated by Gerst and Quay (2001). Recent investigations have confirmed this on samples from the stratosphere, where CH_4 oxidation is the only significant in-situ source and can be studied without interference from the surface sources (Rahn et al., 2003; Röckmann et al., 2003; Rhee et al., 2006). Nevertheless, it is not straightforward to apply those stratospheric results to the troposphere. Basically no information is available on isotope effects for H_2 formation from the oxidation of non-methane hydrocarbons.

In addition to the stratospheric studies, also laboratory studies have investigated the isotope effects in the oxidation chain from CH_4 to H_2 (Gierzak et al., 1997; Feilberg et al., 2004, 2005b, 2007a, b; Rhee et al., 2008; Nilsson et al., 2007, 2010). As usual for isotope effects, the most important fractionations occur where there are branching steps in the reaction mechanism. The series of rate constants of methane and deuterated methanes with OH determined by Gierzak et al. (1997) indicates that the abstraction probability for H and D in CH_3D are 96% and 4%, respectively, so D abstraction is much less than the statistically expected value of 25%. Recent measurements have shown that in the second abstraction step (CH_2DO+O_2), the abstraction probability of D is 11%, again much less than the statistically expected 33% (Nilsson et al., 2007). As D abstraction is much slower than H abstraction, most of the D from the original CH_4 stays in the oxidation chain, whereas the total number of H atoms is reduced by a factor of 2 from CH_4 to H_2. This leads to a strong enrichment in the D/H ratio, and thus the δD value.

The third step where branching occurs is production of H_2 from formaldehyde. Reactions (R1)–(R3) remove formaldehyde, two photolysis channels and the reaction with OH. Only the so-called molecular photolysis channel (R1) produces H_2. Therefore, the fractionation between HCHO and H_2 in the atmosphere depends on the fractionation constant of Reaction (R1) relative to the flux-weighted fractionation in the total removal of HCHO.

$$HCHO + h\nu \rightarrow H_2 + CO \tag{R1}$$

$$HCHO + h\nu \rightarrow H + HCO \tag{R2}$$

$$HCHO + OH \rightarrow H_2O + HCO \tag{R3}$$

The fractionation constant in Reaction (R3) was determined in a laboratory experiment (Feilberg et al., 2004) to be $KIE_{OH} = 1.28\pm0.01$, where KIE is the ratio of rate constants of the non-deuterated and deuterated molecules $KIE=k_H/k_D$. For HCHO photolysis, different studies have reported differing values. Feilberg et al. (2007b) carried out measurements at the European Photoreactor Facility EUPHORE in Valencia, Spain, and found KIEs for the molecular Reaction (R1) and radical Reaction (R2) channel of $KIE_{mol}=1.82\pm0.07$ and $KIE_{rad}=1.1\pm0.06$. Rhee et al. (2008) carried out photolysis experiments in a glass bulb under natural insolation and found $KIE_{mol}=2.00\pm0.04$ and $KIE_{rad}=4.54^{+2.60}_{-1.21}$. Whereas KIE_{mol} values are in reasonable agreement, the values for KIE_{rad} disagree strongly. However, in none of the experiments this KIE_{rad} was measured directly, only inferred. In the case of Feilberg et al. (2007b), the combined KIE_{tot} was determined directly by absorption spectroscopy using D-labeled reaction mixtures. Furthermore, δD of the (extremely enriched, because of the labeled H_2CO precursor) H_2 product was measured by isotope ratio mass spectrometry, and these results were used in a photochemical model to determine KIE_{mol} and KIE_{rad}. Rhee et al. (2008) derived KIE_{mol} from the $\delta D(H_2)$ at small reaction yields, where the second order effect of the radical channel is negligible. They determined KIE_{rad} by total conversion of HCHO and mass balance considerations.

Here we report an independent study of the hydrogen isotope effect in the production of H_2 from HCHO. The experiments were carried out in the SAPHIR atmosphere simulation chamber at Forschungszentrum Jülich under almost ambient conditions and using natural isotope abundance HCHO reactant.

2   Experimental

The experiments were carried out in the atmospheric simulation chamber SAPHIR at Forschungszentrum Jülich, Germany. SAPHIR is a large (5 m diameter, 18 m length, $270\pm10\,m^3$ volume) cylindrical chamber made of double-walled FEP film suspended in a steel frame allowing to study

atmospheric reactions under ambient radiation conditions. At the same time, the gas mixture in the SAPHIR chamber can be carefully selected to study only the reactions of interest. A mixture of N$_2$ and O$_2$ (>99.9999% purity) is used as ultra-clean bath gas. The space between the two Teflon walls of the reactor is constantly flushed with clean N$_2$, thus H$_2$ cannot leak in from outside. Air losses due to consumption by the analytical instruments and small leaks are compensated automatically by a replenishment flow of pure synthetic air (3–4 m^3 h^{-1}) into the chamber maintaining constant pressure (50 Pa above ambient) in the chamber. The dilution rate for trace gases during the experiments is derived from the measured replenishing flow. Photolysis inside the chamber is provided by sunlight. The FEP foil has a high transmission for visible light, UV-A, and UV-B (Bohn et al., 2005), while a roof-system allows fast shadowing of the chamber if required.

During the experiments, the analytics of Forschungszentrum Jülich that are operated at the SAPHIR chamber provided an extensive characterization of the photochemical conditions. Actinic flux spectra were measured outside of SAPHIR with a temporal resolution of about 2 min. The spectra were converted to SAPHIR conditions with a model which leads to minor changes in the relative spectral distributions and an attenuation of typically 25% (Bohn and Zilken, 2005). Three examples of chamber actinic flux spectra for different solar zenith angles are shown in Fig. 1. These actinic flux spectra were then multiplied by the wavelength dependent absorption cross sections and quantum yields from the IUPAC (Atkinson et al., 2006) or JPL recommendations (Sander et al., 2006) to calculate photolysis frequencies for the two HCHO photolysis channels. Temperature, humidity, pressure, ozone, nitrogen oxides, carbon monoxide, hydrocarbons, including several oxygenated species, and of course formaldehyde were measured (e.g. Apel et al., 2008; Bohn et al., 2005; Rohrer et al., 2005; Brauers et al., 2007; Wisthaler et al., 2008).

In our experiments, approximately 500 ppb HCHO, produced by complete evaporation of typically 200 mg paraformaldehyde into the chamber, was used. A weighted amount of solid paraformaldehyde was gently heated with a heat gun until it was pyrolyzed completely into a stream of high purity N$_2$ (>99.999%), which flushed the gaseous HCHO into the chamber. The inlet was heated and flushed with N$_2$ after the pyrolysis was complete to achieve a quantitative injection.

A commercially available instrument (AL4001, Aerolaser GmbH, Garmisch-Partenkirchen, Germany) was used for HCHO measurement. The applied technique transfers gaseous HCHO quantitatively into the liquid phase and derivatizes it via the Hantzsch reaction to yield a dye which is fluorimetrically detected (e.g. Wisthaler et al., 2008). The instrument was calibrated using liquid HCHO standards. The accuracy of the HCHO measurement was 5 % (accounting for the individual 1-σ errors of the slope of the calibration
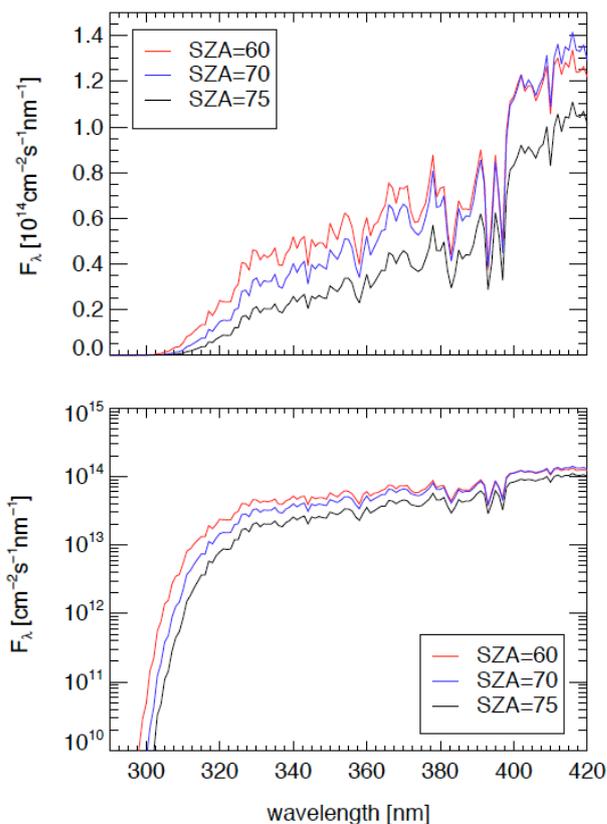

Fig. 1. Three examples of SAPHIR actinic flux spectra for different solar zenith angles (SZA) measured during Experiment 3. Top: linear y-axis scale, bottom: logarithmic y-axis scale.

curve, the flow measurements and the stripping efficiency of HCHO). Zeroing signals were obtained by passing the sampling air through a filter cartridge containing a Hopkalite catalyst.

The HCHO injection procedure has been successfully used, tested and described in previous studies (Brauers et al., 2007; Wisthaler et al., 2008). These studies show that the absolute value and temporal evolution of the HCHO concentration as measured in the SAPHIR chamber can be reproduced very well by the model using the weighted amount of paraformaldehyde added and the known dilution rate (e.g., Fig. 2 of Brauers et al., 2007). This applies also for other trace gases as shown in (Apel et al., 2008). In the present study, the pink model curves in Fig. 2 are based on the weighted amount of HCHO injected, and this yields good agreement with the measurements.

Since the isotope monitoring mass spectrometry technique for the HD measurement requires a minimum of 2.5 nmol H$_2$ for high-quality analysis, 200–400 ppb background H$_2$ were added at the beginning of the experiment. We used two different H$_2$ reference gases with very different isotope composition as background, $\delta D_{bg} = (-177 \pm 5)$‰ and $\delta D_{bg} = (-680 \pm 20)$‰, respectively.
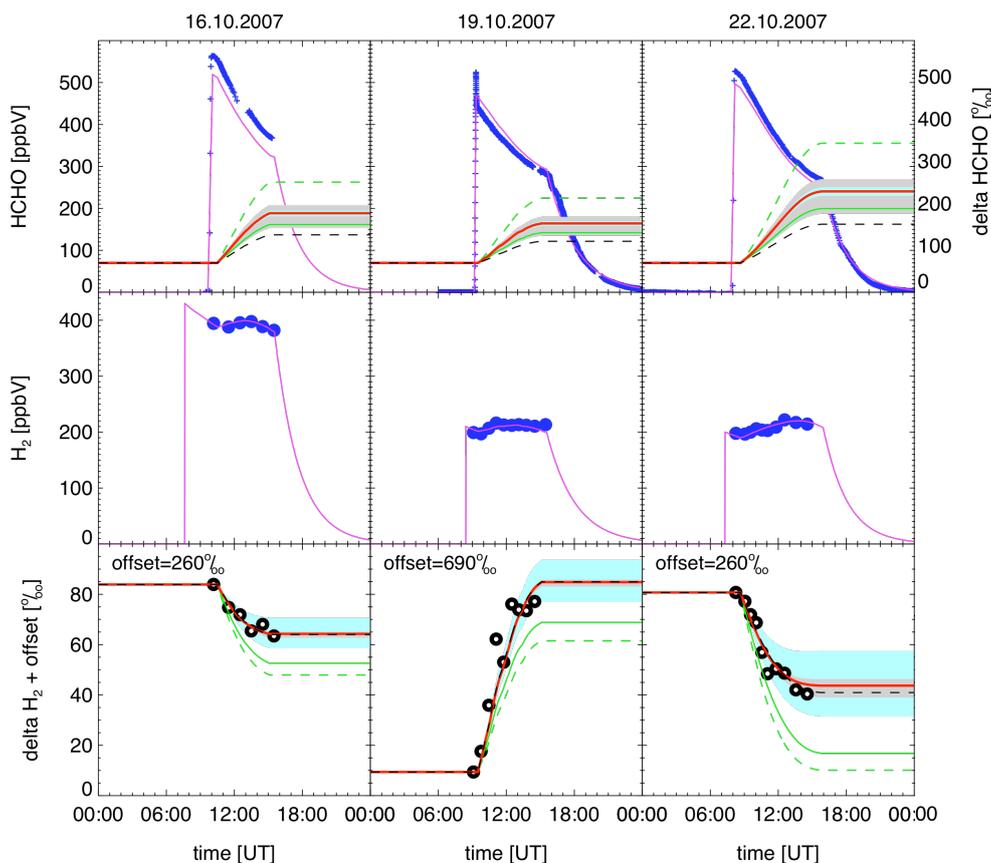
Fig. 2. Experimental and model results of the formaldehyde photolysis experiments in the SAPHIR chamber. Top panels show the concentration (left scale) and isotopic composition (rights scale) of formaldehyde. Middle panels show the H_2 concentration, bottom panels show the isotopic composition of H_2, shifted in positive direction by the listed offsets in order to subtract the effect from the different bath gases used. Symbols represent measurement results (blue: concentration, black: δD). Lines represent model results as follows: pink: concentration; red: δD for $KIE_{rad} = KIE_{mol} = 1.63$ (line 1 in Table 2); grey shaded area: KIE_{rad} varied by ± 0.5; light blue shaded area: KIE_{mol} varied by ± 0.1; black dashed line: $KIE_{rad} = 1.00$, $KIE_{mol} = 1.60$ (line 8 in Table 2); green solid line: Feilberg et al. (2007b); green dashed line: Rhee et al. (2008).

Two control experiments with different gas mixtures were carried out, in which the chamber was not opened to sunlight (Table 1). These control experiments served to confirm that no outside H_2 can enter the chamber through the Teflon foil and to assure stability of the δD value of the background H_2. In the first control experiment (C1, Table 1), 1200 ppb of H_2 were added to the N_2/O_2 bath gas in the chamber. The mixture was sampled every hour for 7 h, then left standing overnight, and sampled again two times on the following day. Samples were taken at the start and after 2, 4 and 6 h. In the second control experiment (C2, Table 1), 350 ppb H_2, 500 ppb HCHO and 500 ppm CO as OH quencher were admitted (see below), thus simulating a real experiment, but without sunlight. Samples were collected at the start and after 2, 4 and 6 h.

In the HCHO photolysis experiments, 500 ppm of CO were added as OH quencher in order to suppress the HCHO+OH reaction. Experiments 1 and 3 were similar ex-

periments with different background mixing ratios of H_2. Experiment was similar to Experiment 3, but in Experiment 2 the background H_2 was provided from a different supply and had a very depleted isotopic composition of $\delta D \approx -680\%$ (see below).

Experiments were usually started at about 10:00 local time and ended around 17:00 local time, after which the chamber was flushed for the experiment on the following day. The H_2 concentration and isotopic composition were measured on flask samples taken at 30–120 min intervals during the experiments. A total of 60 samples were taken by filling 2 L glass flasks (Normag AG) equipped with Kel-F stopcock seats to ~1.9 bar absolute pressure with a KNF Neuberger membrane pump. Flasks were flushed 3 min before sampling. The samples were analyzed within 4 weeks at the isotope laboratory of the Institute for Marine and Atmospheric research Utrecht.

Table 1. List of gas mixtures used in the control and HCHO photolysis experiments.

#	date	$[H_2]$/ppb	$\delta D(H_2)_{bg}$/‰	[HCHO]/ppb	[CO]/ppm	type
1	16.10.	400	-177 ± 5	500	500	photolysis
C1	17/18.10.	1200	-177 ± 5	0	0	control
2	19.10.	200	-680 ± 5	500	500	photolysis
3	22.10.	200	-177 ± 5	500	500	photolysis
C2	25.10.	350	-177 ± 5	500	500	control

The isotopic composition and concentration of H_2 in the air samples was determined by an isotope monitoring mass spectrometry technique based on Rhee et al. (2004) but modified to allow slightly larger samples to be analyzed. The analytical system has been improved such that all valve switching, heating and cooling steps and the flow rate change are automated. An air sample of ≈350 ml is first admitted from the sample flask to a ≈500 ml sample volume of the analytical system. The air is then connected for 10 min to a $6\,cm^3$ stainless steel volume attached to a liquid Helium cold head at ~30 K where the bulk air and most other air constituents condense. The H_2 remains in the gas phase and is subsequently flushed with ultra-clean Helium (20 ml/min) to a $1/8''$ diameter stainless steel pre-concentration trap. This trap is filled with molecular sieve 5Å and immersed into a liquid nitrogen bath, which has been cooled down to the triple point of N_2 (63K) by continuously pumping on the gas phase above the N_2. Pre-concentration takes 20 min, and then the sample is transferred by a 1 ml/min flow of He into a focus trap held at liquid nitrogen temperature. When the sample has been transferred to the focus trap, the flow rate is reduced to $250\,\mu l$/min, the trap is released from the lN_2 bath and the H_2 peak is admitted to an additional Nafion drying unit, the open split interface and finally the isotope ratio mass spectrometer. Ion currents of $m/z=2$ and $m/z=3$ are monitored as voltages across $10^9\Omega$ and $10^{12}\Omega$ resistors on a ThermoFinnigan Delta plus XL isotope ratio mass spectrometer. The sample peak is bracketed by 6 square peaks of the MS running gas (3 before, 3 after the peak) and the running gas peak before the sample peak is assigned as internal reference peak. For referencing we use a stainless steel cylinder filled with whole air by the University of Heidelberg, which is measured routinely at least once per day in the same way as the sample air. The isotopic composition of this air has been calibrated against mixtures of two pure H_2 gases of certified isotopic composition ($\delta D=+200.5$‰ and $\delta D=9.0$‰ vs. VSMOW, respectively, Messer Griesheim), which were diluted in H_2-free air and analyzed the same way as the reference air.

Quantification of the $m/z=2$ peak from a known amount of air allows the mixing ratio to be determined with a reproducibility of 1–2%, which is similar to state-of the art H_2 analyzers. The typical error of the analytical system based on repetitions of reference air measurements is 2–5‰. The iso-topic composition (δD) of the paraformaldehyde stock used for the experiments was determined by Agroisolab, Jülich to be $(+70.0\pm1.4)$‰ versus VSMOW.

3 Photochemical modeling

The research center Jülich operates an advanced photochemical model specifically designed for evaluation and interpretation of SAPHIR experiments (e.g. Rohrer et al., 2005; Karl et al., 2006). Appendix A shows the full list of reactions and rate coefficients included in the SAPHIR model. The model is initialized with the starting concentrations of the reactants and photochemistry is driven by the photolysis frequencies. The isotopically substituted species HDCO and HD have been added to this model and were initialized according to the δD values measured at the beginning of each experiment. The Isotope fractionation factor for reaction of HCHO with OH $KIE_{OH}=k_{HCHO+OH}/k_{HCDO+OH}=1.28\pm0.01$ is available from the literature (Feilberg et al., 2004), but it will be shown below that oxidation of HCHO by OH can be neglected in our experiments. The free parameters in the model are the kinetic isotope effects in the molecular and radical channels of HCHO photolysis, KIE_{mol} and KIE_{rad}, and their values were adjusted to minimize the difference between model and experimental results.

4 Results

4.1 Control experiments

The drop of the H_2 concentration in the two control experiments (Table 1), where the roof of the chamber is not opened is in accordance with the dilution derived from the replenishing flow, which is approximately 3.7%/h. The important result from the control experiments is that the isotopic composition does not exhibit a significant change over a period of several hours, which excludes artifacts from fractionation by dilution or possible wall effects. Furthermore, the experiment where HCHO is added shows the same dilution rate for H_2 and HCHO, thus HCHO is stable in the reaction chamber.
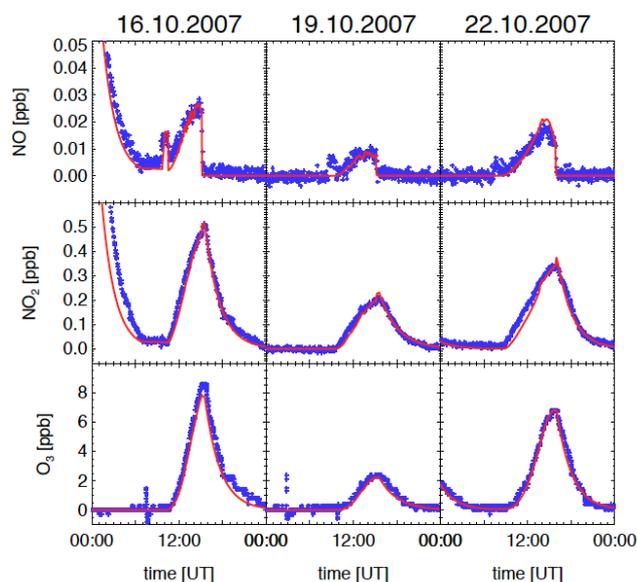
Fig. 3. Comparison of model and measurement results for the photochemically important species NO, NO$_2$ and O$_3$.

Fig. 4. The temporal evolution of HCHO and NO$_2$ photolysis frequencies. Molecular and radical channel photolysis of HCHO are denoted J(HCHO)$_m$ and J(HCHO)$_r$, respectively.

4.2 Photolysis experiments

In the photolysis experiments on 16, 19 and 22 October 2007 (referred to in the following as Experiments 1, 2 and 3, respectively, according to Table 1), HCHO removal starts immediately after the chamber is exposed to sunlight (Fig. 2). 30 to 40% of the initial HCHO is removed during the course of the experiment. The molecular photolysis channel produces H$_2$, whose concentration increases accordingly, despite the continuous dilution. At the same time, the isotopic composition of H$_2$ changes significantly. It should be noted that what is measured is not the isotopic composition of the freshly formed H$_2$, but the mixture of the background reservoir plus the freshly formed fraction. This background reservoir, which is necessary to provide sufficient material for isotope analysis, impedes the direct identification of the freshly produced H$_2$. Therefore, not the absolute δD values, but the changes in δD have to be evaluated to derive the isotopic composition of the H$_2$ produced. When the background reservoir is larger (Experiment 1, [H$_2$]$_{bg}$ = 400 ppb) the isotopic composition changes more slowly than for a smaller background reservoir (Experiment 3, [H$_2$]$_{bg}$ = 200 ppb).

Qualitatively, in Experiment 1 and 3, δD(H$_2$) decreases with time, which shows that the freshly produced fraction is isotopically lighter than the background reservoir. In Experiment 2 with the strongly depleted background reservoir, δD(H$_2$) increases during the experiment, because the freshly produced H$_2$ is enriched relative to the reservoir. In principle, it should be possible to determine the source signature from those experiments by triangulation, but this is not straightforward. Due to the kinetic fractionation, the isotopic
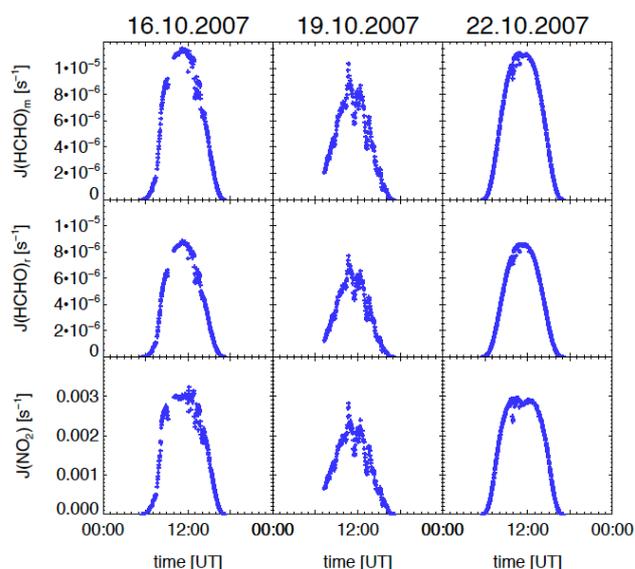
composition of HCHO also changes strongly with increasing degree of removal and we do not have an isotopically constant substrate. Data interpretation was therefore made using the SAPHIR photochemical model.

4.3 Model results

The SAPHIR model is used to interpret and evaluate the photolysis experiments. To demonstrate the performance of the model, Fig. 3 shows a comparison of measured and modeled results for the photochemically important species NO, NO$_2$ and O$_3$. NO and NO$_2$ are not added as gas phase species to the reactor, but are produced by release of HONO from the reactor walls (see Appendix A). HONO is then photolyzed to NO+OH (Appendix A), NO is oxidized by HO$_2$ to NO$_2$ and NO$_2$ photolysis produces O$_3$. The good agreement between model and measurement for these three important species indicates that the model captures well key photochemical reactions, as well as the production of HONO from the wall in the SAPHIR chamber.

To illustrate the combination of measurement data and modeling, Fig. 4 shows the temporal evolution of HCHO and NO$_2$ photolysis frequencies for the three days of photolysis experiments, which are used as input for the SAPHIR model. The HCHO values are already specified for the molecular and the radical channel individually. Each point on this figure is based on an actinic flux spectrum as shown in Fig. 1 and the split-up into molecular and radical channel is according to the IUPAC recommendations for the respective quantum yields in the base model. Integrated over the entire experiment, the total branching ratio between molecular and radical

channel photolysis of HCHO is $\approx 58\% : 42\%$, which is important for the discussion below.

In Fig. 2 the measurements of HCHO mixing ratio, H_2 mixing ratio and $\delta D(H_2)$ are compared to values modeled with the SAPHIR model. In all cases the model captures the evolution of the mixing ratios very well, which is expected since formaldehyde photolysis is well understood as regards changes in concentration.

The new feature in this work is the incorporation of isotope information. HCHO and HCDO are modeled as separate species and the kinetic isotope effects KIE_{mol} and KIE_{rad} in the two photolysis channels of HCHO and HCDO (Reactions R1 and R2) are included and can be adjusted to match the observations.

A potential complication is the interference from the competing reaction of HCHO with OH, which is also associated with isotope fractionation. The experiments were carried out under extremely dry conditions (dew point -55 C) in order to suppress OH formation from the reaction $O(^1D)+H_2O$. Furthermore, a large excess of CO was added to the SAPHIR chamber in order to quench OH radicals. The model results in Fig. 5 show OH and HO_2 concentrations during the experiments. OH levels were kept below 1.5×10^4 cm^{-3}, which means that OH chemistry is indeed negligible in our experiments. The three bottom panels of Fig. 5 show corresponding removal rates of HCHO by the two photolysis channels and reaction with OH. The model calculations confirm that the suppression of OH in the chamber by the excess CO works, removal of HCHO by OH is less than 0.5% of the total removal of HCHO and can be neglected for the interpretation of the data.

A further potential removal process is via the reaction of a $HCHOHO_2$ adduct that isomerizes to $HOCH_2OO$ with HO_2 as described in (Nilsson et al., 2007). To examine the influence of this channel, the reaction system has been extended by the following reactions with rate coefficients from Sander et al. (2006):

$$HCHO + HO_2 \rightarrow HOCH_2O_2 \tag{R4}$$
$$2 \times HOCH_2O_2 \rightarrow 2 \times HCOOH + 2 \times HO_2 \tag{R5}$$
$$HOCH_2O_2 + HO_2 \rightarrow HOCH_2OOH \tag{R6}$$
$$HOCH_2O_2 + HO_2 \rightarrow HCOOH \tag{R7}$$
$$HOCH_2O_2 + HO_2 \rightarrow HOCH_2O + OH \tag{R8}$$
$$HOCH_2O_2 \rightarrow HCHO + HO_2 \tag{R9}$$
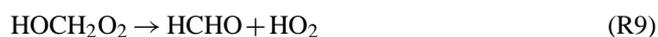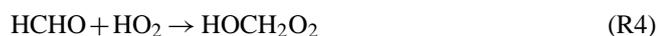
For typical conditions of $[HO_2]= 60 \times 10^8$ cm^{-3} and a HCHO mixing ratio of 500 ppb this leads to concentrations of the adduct of $[HOCH_2O_2]= 3 \times 10^7$ cm^{-3}, and the removal rates by this process are less than 1% of the total removal. The important point is that the adduct dissociates with a time constant of 150 s^{-1} into the reactants and therefore this process can be neglected in the analysis. It should be noted that
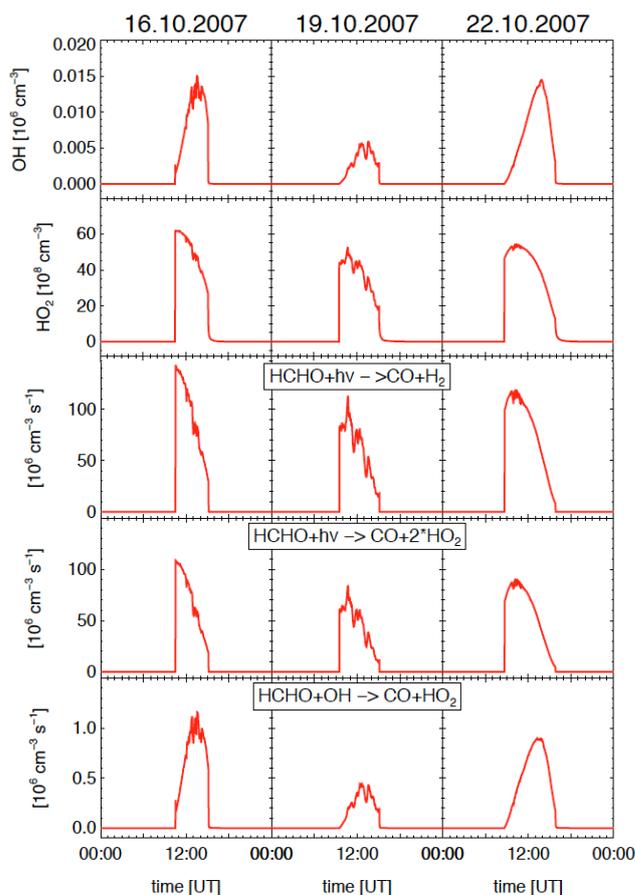
Fig. 5. Modelled OH and HO_2 mixing ratios in the SAPHIR chamber, and the calculated removal rates of HCHO via the two photolysis channels and reaction with OH. Removal by OH accounts for <0.5% of the total removal and can be neglected.

this is only valid if no hydrogen isotope exchange occurs via formation and dissociation of the adduct.

In addition to these HCHO removal processes, it has also been investigated whether a contamination of HCHO that is produced from the walls of the SAPHIR chamber can affect the results. Wall production of HCHO is well established and occurs at a rate of typically 0.75 ppb/hr. This means that after typically 6 h of experiment, 6 ppb of wall HCHO have been added to the reaction mixture, <2% of the total reservoir at the end of the experiment. Only a small fraction of this HCHO would have been converted to H_2. We have included the wall source with a wide range of δD values (0–300‰) in the model calculations below and this changes the optimized KIE values by less than 0.002, so wall production also can be neglected in the analysis.

These initial model calculations show that the only significant HCHO loss processes are the photolysis into the molecular and radical channel, respectively, and the measurements can be used to determine the kinetic isotope effects without

Table 2. χ^2 values for a range of $KIE_{mol}-KIE_{rad}$ pairs.

	IUPAC		
Constraint	KIE_{mol}	KIE_{rad}	χ^2
$KIE_{mol}=KIE_{rad}$	1.63	1.63	34.3
JPL quantum yields*	1.64	1.64	42.6
$KIE_{mol}=1.64$, $KIE_{rad}=1.63$	1.64	1.63	34.7
$KIE_{mol}=1.65$, $KIE_{rad}=1.63$	1.65	1.63	35.9
$KIE_{mol}=1.66$, $KIE_{rad}=1.63$	1.66	1.63	37.7
$KIE_{mol}=1.62$, $KIE_{rad}=1.63$	1.62	1.63	34.6
$KIE_{mol}=1.61$, $KIE_{rad}=1.63$	1.61	1.63	35.7
$KIE_{mol}=1.60$, $KIE_{rad}=1.63$	1.60	1.63	37.6
JPL quantum yields*	1.69	1.63	43.4
$KIE_{rad} \geq 1$	1.60	1.00	31.8
Feilberg et al. (2007b)	1.82	1.10	170
JPL quantum yields*	1.82	1.11	204
Rhee et al. (2008)	2.00	4.50	321
JPL quantum yields*	2.00	4.50	403
$KIE_{rad}=1.00$	1.60	1.00	31.8
$KIE_{rad}=2.00$	1.64	2.00	35.3
$KIE_{rad}=4.00$	1.66	4.00	37.7
$KIE_{rad}=6.00$	1.67	6.00	38.6

*: Same constraint as line above, but calculated with JPL quantum yields for HCHO photolysis into radical and molecular channel, respectively instead of IUPAC quantum yields.

interference from other reactions. It should be noted that the system is underdetermined, since we only have one measurable, $\delta D(H_2)$ but two unknowns, KIE_{mol} and KIE_{rad}. Therefore, we can in principle only determine pairs of KIE_{mol} and KIE_{rad}.

4.4 Isotope modeling

As first attempt, we choose $KIE_{mol}=KIE_{rad}=KIE$. This initial choice is made only for convenience and it is in contrast to recent publications that indicate strong (but not consistent among publications) differences between KIE_{mol} and KIE_{rad}. The value of KIE is then optimized by minimizing the squared sum of model-data differences for all 26 measurement points from the three photolysis experiments that are included in the analysis, $\chi^2 = \sum_{i=1}^{26} \left(\delta D_{meas,i} - \delta D_{mod,i} \right)^2$. Table 2 shows that the best fit to the results of the three photolysis experiments is achieved for $KIE_{mol}=KIE_{rad}=1.63$, which is displayed as the red solid line in Fig. 2. For this value, $\chi^2=34.3$, i.e., the typical difference between the measurements and the model, $\chi=5.9‰$ is very similar to the estimated analytical uncertainty in δD of $\approx 5‰$.

We can exploit the model-measurement differences χ^2 to obtain a first estimate of an error bar in KIE. Based on 26 individual measurements, χ^2 has a statistical error of $\chi^2/26=1.3$. Consequently, KIE values that produce χ^2 val-

ues up to 35.6 still fall in the range of valid scenarios. Table 2 shows that this leads to a result of KIE$=1.63\pm0.02$ for the case $KIE_{mol}=KIE_{rad}$.

Figure 2 also shows the different sensitivity of the model results to changes in KIE_{mol} and KIE_{rad}. The cyan area depicts the range of model results when KIE_{mol} is changed by ±0.1 while KIE_{rad} remains unchanged, the grey area the range of model results when KIE_{rad} is changed by ±0.5 while KIE_{mol} remains unchanged. The effects on the modeled $\delta D(HCHO)$ roughly scale with the changes in the KIEs, which leads to a ≈5 times larger change of $\delta D(HCHO)$ when KIE_{rad} is changed by the 5 times larger value. Both channels have a similar effect on changes of $\delta D(HCHO)$ because they both remove HCHO at comparable rates (58% : 42%). For the H_2 production, however, the change in $\delta D(H_2)$ caused by the modeled change in KIE_{rad} is 5 times smaller compared to the change caused by a modeled change in KIE_{mol}, although the change in KIE_{rad} is 5 times larger than the change in KIE_{mol}. This is due to the fact that KIE_{mol} has a direct effect on $\delta D(H_2)$, whereas KIE_{rad} only changes $\delta D(H_2)$ through a feedback via $\delta D(HCHO)$ as discussed below in more detail. The poor sensitivity to KIE_{rad} means that it is not possible to strongly constrain KIE_{rad} by our measurements. On the other hand, it means that the fact that the system is underdetermined does not pose a strong restriction on deriving precise values for KIE_{mol}. Even when KIE_{rad} is varied over a wide range, this has only a minute effect on the value of KIE_{mol} that is needed to obtain best agreement with the data for a particular KIE_{rad}. Therefore, the insensitivity to KIE_{rad} actually means that we can derive tight constraints on KIE_{mol}.

In retrospect, it is unfortunate that not more samples were taken before starting and after finishing the photolysis period. Determining those points with a higher precision may have enabled an even more precise determination of the total isotope change, and thus KIE_{mol}. Nevertheless, the error estimates are sufficiently low to conclude that for the assumption $KIE_{mol}=KIE_{rad}$ the derived KIE$=1.63\pm0.02$, which is significantly lower than the values reported by Feilberg et al. (2007b) and Rhee et al. (2008).

As mentioned above, both prior studies indicated that there might be large differences between KIE_{mol} and KIE_{rad}. However, there is a large discrepancy in the magnitude of the differences, and there is not even agreement on whether KIE_{mol} is larger or smaller than KIE_{rad}. Therefore, in the second step, we investigate whether the comparatively low value for KIE_{mol} that we have derived above is biased by the arbitrary condition $KIE_{mol}=KIE_{rad}$ made above.

When both KIE values are optimized simultaneously, KIE_{rad} yields values<1. This is not supported by any of the prior studies and we constrain KIE_{rad} to be ≥1. In this case, the best fit is obtained for $KIE_{rad}=1$ and $KIE_{mol}=1.60$. The χ^2 value for this scenario is the lowest with $\chi^2=31.8$ (Table 2). This scenario is also shown in Fig. 1 as dashed black line, which is very similar and in some cases virtually indistinguishable to the optimal solution for $KIE_{mol}=KIE_{rad}$.

Since $KIE_{mol} = 1.60$ is the optimum valued for $KIE_{rad} \geq 1$, we extend our first error estimate to the value of $KIE_{mol} = 1.63 \pm 0.03$ to account for possible differences between KIE_{mol} and KIE_{rad}.

It is interesting, and maybe counterintuitive, that both KIEs are shifted in the same direction when adjusted independently. KIE_{mol} directly influences the isotopic composition of the product H_2, and when KIE_{mol} is decreased, $\delta D(H_2)$ increases accordingly. KIE_{rad}, on the other hand, has only an indirect effect by changing the isotopic composition of the formaldehyde reservoir that remains for H_2 formation. At the start of the experiment changing KIE_{rad} has no effect at all. In the course of the experiment, smaller values of KIE_{rad} (i.e., relatively faster HCDO removal via the radical channel) lead to a decrease of $\delta D(HCHO)$ in the remaining formaldehyde reservoir. To make up for the lower $\delta D(HCHO)$ value, KIE_{mol} also has to be decreased in the model to still explain the same $\delta D(H_2)$ value. This explains the fact that optimized pairs of KIE_{mol} and KIE_{rad} are either both higher or both lower than the value of 1.63 found for $KIE_{mol} = KIE_{rad}$.

Based on these theoretical considerations, it can already be deduced that it is impossible to quantitatively reconcile the results of Feilberg et al. (2007b) with the new dataset, as KIE_{mol} from Feilberg et al. (2007b) is significantly larger and KIE_{rad} significantly smaller than the new values derived for $KIE_{mol} = KIE_{rad}$. The $KIE_{rad} = 1.10$ derived in Feilberg et al. (2007b) would require a KIE_{mol} at the low end of the error range (≈ 1.60), even increasing the discrepancy of our best estimated to the KIE_{mol} determined in Feilberg et al. (2007b). Concerning the results by Rhee et al. (2008) KIE_{rad} and KIE_{mol} deviate in the same direction, but the differences are also much larger. Even the extreme value of $KIE_{rad} = 4.5$ is not sufficient to compensate for the only slightly higher value of $KIE_{mol} = 2.0$ because of the lack in sensitivity to KIE_{rad}. The third group of values in Table 2 shows optimized values of KIE_{mol} for a wide range of KIE_{rad} values (between 1 and 6). Even for these extreme cases, the optimized KIE_{mol} only varies between 1.60 and 1.66. Also, the χ^2 value increases with increasing values for KIE_{rad} and KIE_{mol}, thus lower values are more likely. Fig. 2 also shows model results obtained with the parameters from Feilberg et al. (2007b) and Rhee et al. (2008), and it is clear that they do not yield satisfactory agreement with the observations.

An independent error estimate for KIE_{mol} is derived by determining the sensitivity of the optimized KIE values to variations in other experimental parameters. The results are summarized in Table 3. For the most important starting parameters, i.e. the initial mixing ratio and initial isotopic composition of the HCHO and H_2 reservoirs, the reported errors represent the total error of 3 model runs where the respective parameters were changed in all three experiments independently. In our experimental setup, the results are relatively insensitive to changes in these parameters due to the "isotope triangulation" approach. For example, a 5% higher ini-

Table 3. Sensitivity of optimized KIE_{mol} values to changes in important reaction parameters. KIE_{rad} is always fixed at 1.63.

Constraint	$\Delta(KIE_{mol})$
[HCHO]$_0$ changed by 5%	± 0.012
[H$_2$]$_0$ changed by 5%	± 0.011
$\delta D(HCHO)_0$ changed by 10‰	± 0.014
$\delta D(H_2)_0$ changed by 4‰	± 0.028
Include wall source of HCHO, ($\delta D = 0 - 300$‰)	$\pm 0.001^a$
Uncertainty in branching ratio, JPL-IUPAC^b	$+0.01$
Uncertainty in KIE_{rad} (1.00–2.00)^c	$-0.03, +0.01$
Total error	$-0.046, +0.038$

^{a} maximum for deviation the case $\delta D(HCHO) = 0$‰.
^{b} from examples in Table 2.
^{c} from Table 2 for the range $1 \leq KIE_{rad} \leq 2$.

tial mixing ratio of HCHO means that relatively more H_2 is formed from HCHO. In the experiment with the enriched background H_2, this results in an additional depletion during the course of an experiment, because more depleted H_2 is added in the model. If only this experiment was evaluated, a smaller KIE_{mol} would compensate for this change. However, we simultaneously optimize all experiments, also the one with the isotopically depleted bath gas. For this experiment, the additional H_2 results in an additional enrichment, and a now larger KIE_{mol} is needed to compensate for the change. Thus, the triangulation approach strongly attenuates the sensitivity of KIE_{mol} to changes in the initial conditions and allows deducing a robust estimate of KIE_{mol}. The system is most sensitive to changes in the initial isotopic composition of the H_2 reservoir, and this error is 0.028‰ for a 4‰ change in $\delta D[H_2]_{bg}$.

In addition to the changes in initial condition, we include in the total error estimate the effect of the wall source of HCHO of 0.75 ppb/h (see above), where we performed model calculations for four different values of isotopic composition of this HCHO (0, 100, 200, 300‰) spanning the range of values modeled for the experiments (Fig. 2). The largest deviation in KIE_{mol} observed when this source is included was 0.001, so it is effectively negligible.

Furthermore, we include the error due to the uncertainty in the branching ratios between the molecular and radical channel from the IUPAC and JPL evaluations of 0.01 (see below and Table 2) and the error from the uncertainty in KIE_{rad} where we include the range between 1.00 and 2.00, since for larger variations the χ^2 value increases strongly, indicating poor agreement with the measurements (Table 2). This leads to an error range of -0.03 to $+0.01$.

Summing up all errors independently leads to $KIE_{mol} = 1.63^{+0.038}_{-0.046}$ for the kinetic isotope effect in the molecular photolysis channel from the experiments conducted in this study.

The SAPHIR model also calculates δD(HCHO), which could not be determined experimentally. δD(HCHO) values increase by ~100 to 200‰ in the model, depending on the relative removal fraction. These are large changes and although it appears to be very difficult to obtain high precision in isotope measurements on HCHO, the precision achieved in the only publication that is available to date (±50‰; Rice and Quay, 2006) would be sufficient to detect changes of this magnitude.

4.5 Discussion

It is intriguing that three different studies of the KIEs in the photolysis of formaldehyde yield three different results. Therefore, in the following we attempt to explain the differences. We first recall the relation between KIE$_{mol}$, KIE$_{rad}$ and KIE$_{tot}$. β_{mol} and β_{rad} are the relative photolysis yields of the molecular and radical channel, respectively, and for near-natural isotope abundance, β_{mol} and β_{rad} can be approximated by the branching ratios for the non-deuterated HCHO molecules. In this case

$$\frac{1}{\text{KIE}_{tot}} = \frac{J_{HDCO}}{J_{HHCO}}$$

$$= \frac{J_{HDCO \to HD+CO} + J_{HDCO \to H+DCO} + J_{HDCO \to D+HCO}}{J_{HHCO \to HH+CO} + J_{HHCO \to H+HCO}}$$

$$= \frac{J_{HDCO \to HD+CO}}{J_{HHCO \to HH+CO} + J_{HHCO \to H+HCO}}$$

$$+ \frac{J_{HDCO \to H+DCO} + J_{HDCO \to D+HCO}}{J_{HHCO \to HH+CO} + J_{HHCO \to H+HCO}}$$

$$= \frac{J_{HDCO \to HD+CO}}{J_{HHCO \to HH+CO}} \times \frac{J_{HHCO \to HH+CO}}{J_{HHCO \to HH+CO} + J_{HHCO \to H+HCO}}$$

$$+ \frac{J_{HDCO \to H+DCO} + J_{HDCO \to D+HCO}}{J_{HHCO \to H+HCO}}$$

$$\times \frac{J_{HHCO \to H+HCO}}{J_{HHCO \to HH+CO} + J_{HHCO \to H+HCO}}$$

$$= \frac{1}{\text{KIE}_{mol}}\beta_{mol} + \frac{1}{\text{KIE}_{rad}}\beta_{rad}$$

$$= \frac{1}{\text{KIE}_{mol}}\beta_{mol} + \frac{1}{\text{KIE}_{rad}}(1 - \beta_{mol})$$

Solving for β_{mol} with the KIE values from Feilberg et al. (2007) returns $\beta_{mol} = 0.77$. Whereas there are still considerable uncertainties in radical and molecular channel quantum yields between the IUPAC and JPL recommendations (IUPAC: $\beta_{mol} \approx 0.56$, JPL: $\beta_{mol} \approx 0.63$ for typical atmospheric conditions) (Sander et al., 2006; Atkinson et al., 2006) both values imply a considerable lower value for the molecular channel. This indicates an overestimate of the molecular photolysis channel in Feilberg et al. (2007). The implications of a potential overestimate of β_{mol} for the determination of KIE$_{mol}$ and KIE$_{rad}$ can be qualitatively assessed.

The experiments of Feilberg et al. (2007) were carried out with strongly labeled formaldehyde. If β_{mol} is overestimated, this means effectively that HD production is overestimated compared to the present study. To compensate for the higher flux into the molecular channel, KIE$_{mol}$ needs to be increased and KIE$_{rad}$ decreased. The result is that relatively less D is directed into the molecular channel, which counteracts the higher $\beta_{mol} = 0.77$. Note that due to analytical problems, no concentration data were available for the Feilberg et al. experiments, so that the flux into the molecular channel could not be quantified by H$_2$ measurements. Whereas the discrepancy in the calculated branching ratios between the two studies should be investigated in detail, the effect outlined above may resolve at least part of the deviations between Feilberg et al. (2007) and the present study.

Table 2 also lists the results of the present experiments when instead of the IUPAC recommendations for the branching ratio between the molecular and radical channels, the JPL recommendations are used. The results only change by 0.01 and a sensitivity analysis showed that this is largely due to the "triangulation" approach in the experiments. As the H$_2$ formed is isotopically between the light and heavy reservoirs, it can be constrained very robustly. Changes that would tend to make the model results either heavier or lighter for a single reservoir gas (by compensation of e.g. branching ratio and KIE as explained above) lead to large discrepancies for the experiment with the other H$_2$ reservoir. The freshly produced H$_2$ has to have a well-defined isotopic composition in between the two reservoirs. Finally, the higher values of χ^2 for the optimizations using the branching ratios from JPL indicate that the IUPAC values are in slightly better agreement with our experimental results, but the experiments are not really designed to distinguish these differences.

Rhee et al. (2008) conducted formaldehyde photolysis experiments in 0.1 to 3 L glass or quartz photochemical reactors, employing HCHO mixing ratios between 0.4 and 3 ppm and photolysis times between 1 h and 17 days. Although stability was verified in one experiment for 2 days, the affinity of formaldehyde to stick to surfaces constitutes a potential source of error in these experiments. Furthermore, no radical quencher was used, and the interference from radical reactions was only determined using a model, but without direct supporting measurements of fast photochemistry. A third important uncertainty is that the isotopic composition of the original HCHO was not determined independently. Rather, it was inferred from the H$_2$ product after complete photolysis of pure HCHO to H$_2$ with a mercury photolysis lamp, under the assumption that the HCHO is quantitatively converted to H$_2$. This means that in the absence of other reactants, also the products from the radical channel H and HCO recombine to form H$_2$. This was postulated by (McQuigg and Calvert, 1969), but it is possible that radical reactions with molecules adsorbed at the reactor surface constitute another loss process. Also H$_2$O$_2$ can be formed in the presence of O$_2$ via HO$_2$.

Whereas the partitioning between KIE_{mol} and KIE_{rad} in Feilberg et al. (2007) may be affected by the branching ratios of 77%:23% between the molecular and radical channel, respectively, the value of $KIE_{tot} = 1.58 \pm 0.03$ was directly measured by FTIR spectroscopy in a relative rate experiment using highly enriched HCHO-HCDO mixtures and is considered a robust measurement result. The value of $KIE_{mol} = 1.63^{+0.038}_{-0.046}$ derived above agrees within the combined error bars with the value of 1.58 ± 0.03 from Feilberg et al. (2007b). This indicates that the value of KIE_{rad}, which must account for the difference, may not be as different from KIE_{mol} as concluded in prior studies. Exploring the best estimates and combined error ranges of KIE_{tot} from Feilberg et al. (2007b) and KIE_{mol} from the present study leads to a value of $KIE_{rad} = 1.51^{+0.13}_{-0.15}$.

It is important to note that this estimate is derived from combining results from two experiments that were done under different photochemical and experimental conditions. The Feilberg et al. (2007b) experiments were carried out at the photochemical reactor EUPHORE in Valencia, Spain, in late spring, and with isotopically labeled material.

A precise determination of the KIEs in both photolysis channels is very important for the evaluation of the global isotope budget of molecular hydrogen (Gerst and Quay, 2001; Röckmann et al., 2003; Rhee et al., 2008; Feilberg et al., 2007b, 2005a, 2007a; Price et al., 2007). Even disregarding the feedback via the radical channel, a change of KIE_{mol} from 1.82 to 1.63 implies that the isotopic composition of H_2 from HCHO photolysis decreases by 117‰ ($1.63^{-1}/1.82^{-1} - 1$). This is a huge change, given that photochemistry via HCHO constitutes about 50% of the global H_2 source. Pieterse et al. (2009) already noted that in a simple box model of the isotopic composition of atmospheric H_2, it was difficult to close the isotope budget with the original values from Feilberg et al. (2007b). It was necessary to decrease the difference between KIE_{mol} and KIE_{rad} in order to close the budget. This is confirmed by new calculations with the global chemical tracer model TM5 (Pieterse et al., 2010), where also the pressure effect of KIE_{mol} has been included (Nilsson et al., 2010). The isotope budget is much better closed when the parameterization of the pressure dependence is constrained to the value $KIE_{mol} = 1.63$ at atmospheric pressure that is derived here. If the value of 1.82 is used, the modeled isotopic composition of atmospheric H_2 is far too depleted, which would imply a large uncertainty in other parts of the H_2 budget.

In summary, the present study presents a well-constrained value for KIE_{mol}. Together with KIE_{tot} from Feilberg et al. (2007b), this implies a rather small difference between KIE_{mol} and KIE_{rad}, confirming the suggestion by Pieterse et al. (2009). The model calculations show that direct determination of $\delta D(HCHO)$ would help constraining both fractionation factors from a single photolysis experiment with non-labeled formaldehyde. However, δD measurements on formaldehyde are difficult, and the only published technique for atmospheric $\delta D(HCHO)$ reached a precision of $\pm 50‰$ only (Rice and Quay, 2006), which is of the order of the modeled differences between the scenarios in Fig. 2. Thus, at this precision, such an experiment may not allow a very precise quantification.

5 Conclusions

Three formaldehyde photolysis experiments have been carried out in the SAPHIR atmosphere simulation chamber to determine the associated isotope effects. This was the first study where both, large reactor volumes and near-natural isotope abundance were employed. Similar results are obtained when using two isotopically different H_2 gases as background. Our results allow to closely constrain the kinetic isotope effect in the molecular photolysis channel (KIE_{mol}) to $1.63^{+0.038}_{-0.046}$. With the present experiments, the kinetic isotope effect in the radical channel (KIE_{rad}) cannot be constrained, because H_2 is not formed in this channel and the results are not sensitive to the indirect effect via the effect on the HCHO reservoir. The value for $KIE_{mol} = 1.63^{+0.038}_{-0.046}$ determined here is close to the reported total kinetic isotope effect $KIE_{tot} = 1.58 \pm 0.03$ from Feilberg et al. (2007b), in contrast to the results from Feilberg et al. (2007b) and Rhee et al. (2008). So if KIE_{mol} from this study is combined with KIE_{tot} from Feilberg et al. (2007b), mass balance requires that KIE_{rad} is also not as different at atmospheric surface pressure as concluded in the prior studies. Some of the discrepancy between the results from different research groups appears to result from discrepancies in the branching ratios between the molecular and radical channel of HCHO photolysis.

Appendix A

Table A1. List of reactions included in the SAPHIR photochemical model. Rate coefficients are from (Sander et al., 2006).

reaction		parameter definition	k(298 K) or comment
$H_2O_2+h\nu$	$\rightarrow 2\times OH$	CONST(jh2o2)	observed
$HCHO+h\nu$	$\rightarrow CO+2\times HO_2$	CONST(jhchor)	observed
$HCHO+h\nu$	$\rightarrow CO+H_2$	CONST(jhchom)	observed
$HCDO+h\nu$	$\rightarrow CO+2\times HO_2$	CONST(jhchor/kIE_r)	observed
$HCDO+h\nu$	$\rightarrow CO+HD$	CONST(jhchom/kIE_m)	observed
$HNO_2+h\nu$	$\rightarrow NO+OH$	CONST(jhono)	observed
$HNO_3+h\nu$	$\rightarrow NO_2+OH$	PHTFKT(9.312D$-$07, 1.230, $-$0.307)	scaled to jno2
$HNO_4+h\nu$	$\rightarrow 0.65\times HO_2+0.65\times NO_2$ $+0.35\times NO_3+0.35\times OH$	CONST(3.17E-6$\times$jno2/6e-3)	scaled to jno2
$NO_2+h\nu$	$\rightarrow NO+O$	CONST(jno2)	observed
$NO_3+h\nu$	$\rightarrow NO+O_2$	PHTFKT(2.485D-02, 0.168, $-$0.108)	scaled to jno2
$NO_3+h\nu$	$\rightarrow NO_2+O$	PHTFKT(1.747D-01, 0.155, $-$0.125)	scaled to jno2
$O_3+h\nu$	$\rightarrow O+O_2$	PHTFKT(4.775D-04, 0.298, $-$0.080)	scaled to jno2
$O_3+h\nu$	$\rightarrow O^1D+O_2$	CONST(jo1d)	observed
$WALL+h\nu$	$\rightarrow HNO2$	CONST(4.75 $\times$4.7e13$\times$jno2$\times$ $(1+(RH/11.6)\times(RH/11.6))\times\exp(-3950/T))$	scaled to jno2
$2\times HO_2$	$\rightarrow H_2O_2+O_2$	CONST(3.5E-13$\times$exp(430/T)+1.7E-33$\times$exp(1000/T)$\times$M)	2.70e-012
$2\times NO+O_2$	$\rightarrow 2\times NO_2$	ARRH(3.3E-39, 530.0)	1.95e-038
$2\times NO_3$	$\rightarrow 2\times NO_2+O_2$	ARRH(8.5E-13, $-$2450.0)	2.28e-016
$CO+OH$	$\rightarrow CO_2+HO_2$	ATROE (1.5e-13, $-$0.6, 2.1e9, $-$6.1)	1.40e-013
H_2+OH	$\rightarrow H_2O+HO_2$	ARRH (2.8E-12, $-$1800.0)	6.67e-015
$H_2O+2\times HO_2$	$\rightarrow H_2O+H_2O_2+O_2$	CONST(3.22E-34$\times$exp(2800/T)+2.38E-34$\times$exp(3200/T)$\times$1E-20$\times$M)	6.62e-030
H_2O+O^1D	$\rightarrow 2\times OH$	ARRH(1.63E-10, 60.0)	1.99e-010
H_2O_2+OH	$\rightarrow H_2O+HO_2$	CONST(1.8e-12)	1.80e-012
$HCDO+OH$	$\rightarrow CO+H_2O+HO_2$	ARRH(5.5e-12/1.28,125)	6.54e-012
$HCHO+OH$	$\rightarrow CO+H_2O+HO_2$	ARRH(5.5e-12, 125) 8.37e-012	
$HD+OH$	$\rightarrow H_2O+HO_2$	ARRH(2.8E-12/1.65, $-$1800.0)	4.04e-015
HNO_2+OH	$\rightarrow H_2O+NO_2$	ARRH(1.8E-11,-390.0)	4.86e-012
HNO_3+OH	$\rightarrow H_2O+NO_3$	CONST(2.4E-14$\times$exp(460/T)+6.5E-34$\times$exp(1335/T) $\times$M/(1+(6.5E-34$\times$exp(1335/T)$\times$M)/(2.7E-17$\times$exp(2199/T)))) $(1+(6.5$E-34$\times$exp(1335/T)$\times$M)/(2.7E-17$\times$exp(2199/T)))$	1.54e-013
HNO_4+OH	$\rightarrow H_2O+NO_2+O_2$	ARRH(1.3E-12, 380.0)	4.65e-012
HNO_4	$\rightarrow HO_2+NO_2$	ETROE(2.1E-27, 10900.0, 2.0E-31, 3.4, 2.9E-12, 1.1)	7.12e-002
HO_2+NO	$\rightarrow NO_2+OH$	ARRH(3.5e-12, 250)	8.10e-012
HO_2+NO_2	$\rightarrow HNO_4$	TROE(2.0E-31, 3.4,2.9E-12, 1.1)	1.15e-012
HO_2+NO_3	$\rightarrow 0.3\times HNO_3+0.7$ $\times NO_2+O2+0.7\times OH$	CONST(3.5E-12)	3.50e-012
HO_2+O_3	$\rightarrow 2\times O_2+OH$	ARRH(1.0E-14, $-$490.0)	1.93e-015
HO_2+OH	$\rightarrow H_2O+O_2$	ARRH(4.8E-11, 250.0)	1.11e-010
N_2+O^1D	$\rightarrow N_2+O$	ARRH(2.15E-11, 110.0)	3.11e-011
N_2O_5	$\rightarrow NO_2+NO_3$	ETROE(2.7E-27, 11000.0, 2.0E-30, 4.4, 1.4E-12, 0.7)	4.07e-002
$NO+NO_3$	$\rightarrow 2\times NO_2$	ARRH(1.5E-11, 170.0)	2.65e-011
$NO+O$	$\rightarrow NO_2$	TROE(9.0E-32, 1.5, 3.0E-11, 0.0)	1.68e-012
$NO+O_3$	$\rightarrow NO_2+O_2$	ARRH(3.0E-12, $-$1500.0)	1.95e-014
$NO+OH$	$\rightarrow HNO_2$	TROE(7.0E-31, 2.6, 3.6E-11, 0.1)	7.47e-012
NO_2+NO_3	$\rightarrow N_2O_5$	TROE(2.0E-30, 4.4, 1.4E-12, 0.7)	1.18e-012
NO_2+NO_3	$\rightarrow NO+NO_2+O_2$	ARRH(4.5E-14, $-$1260.0)	6.56e-016
NO_2+O	$\rightarrow NO+O_2$	ARRH(5.1E-12, 210.0)	1.03e-011
NO_2+O	$\rightarrow NO_3$	TROE(2.5E-31, 1.8, 2.2E-11, 0.7)	3.32e-012
NO_2+O_3	$\rightarrow NO_3+O_2$	ARRH(1.2E-13, $-$2450.0)	3.23e-017
NO_2+OH	$\rightarrow HNO_3$	TROE(1.8E-30, 3.0, 2.8E-11, 0)	1.07e-011

Table A1. Continued.

reaction		parameter definition	k(298 K) or comment
NO$_3$+OH	→HO$_2$+NO$_2$	CONST(2.2E-11)	2.20e-011
O+O$_2$	→O$_3$	CONST(6.0E-34×M×(T/300)@(−2.4))	1.52e-014
O+O$_3$	→2×O$_2$	ARRH(8.0E-12, −2060.0)	7.96e-015
O^{1}D+O$_2$	→O+O$_2$	ARRH(3.3E-11, 55.0)	3.97e-011
O$_3$+OH	→HO$_2$+O$_2$	ARRH(1.7E-12, −940.0)	7.25e-014
QH$_2$	→H$_2$	CONST(QH$_2$)	obs. source strength at injection time
QH$_2$	→HD	CONST(QH$_2$×SMOW×(1+IE(QH$_2$)/1000))	obs. source strength at injection time
QHCHO	→HCHO	CONST(QHCHO)	obs. source strength at injection time
QHCHO	→HCDO	CONST(QHCHO×SMOW×(1+IE(QHCHO)/1000))	obs. source strength at injection time
X	→	CONST(Fl/V/3600)	observed dilution for all species

ARRH = FUNCTION[%1×exp(%2/T)]

TROE = FUNCTION[M×%1×(T/300.)@((−1.)×(%2))/(1.+M×%1×(T/300.)@((−1.)×(%2))/(%3×(T/300.)@((−1.)×(%4))))×0.6@(1./(1.+(log10(M×%1×(T/300.) @ ((−1.)×(%2))/(%3×(T/300.)@((−1.)×(%4)))))××2))]

ATROE = FUNCTION[%1×(T/300.)@((−1.)×(%2))/(1.+%1×(T/300.)@ ((−1.)×(%2))/(%3×(T/300.)@((−1.)×(%4))/M))×0.6@(1./ (1.+(log10(%1×(T/300.)@((−1.)×(%2))/(%3×(T/300.)@((−1.)×(%4))/M)))××2))]

ETROE = FUNCTION[((M×%3×(T/300.)@((−1.)×%4)/(1.+M×%3×(T/300.)@((−1.)×%4)/(%5×(T/300.)@((−1.)×%6)))×0.6@(1./(1.+(log10(M×%3×(T/300.)@((−1.)×%4)/(%5×(T/300.)@((−1.)×%6))))××2)))/(%1×exp(%2/T)))]

LNO2 = 1.165D-02

MNO2 = 0.244

NNO2 = −0.267

PHTFKT = FUNCTION[((%1× ((AMAX(COSX,0.01))@%2)×EXP(%3/AMAX(COSX,0.01)))× (AMIN((jno2/(LNO2×((AMAX(COSX, 0.01)) @MNO2)×exp(NNO2/AMAX(COSX,0.01)))), 1.)))]

V = volume of SAPHIR = 270 m^3

Fl = observed purge gas flow of SAPHIR in m^3/h

SMOW: D/H ratio of Standard Mean Ocean Water

References

Apel, E. C., Brauers, T., Koppmann, R., Bandowe, B., Bossmeyer, J., Holzke, C., Tillmann, R., Wahner, A., Wegener, R., Brunner, A., Jocher, M., Ruuskanen, T., Spirig, C., Steigner, D., Steinbrecher, R., Alvarez, E. G., Muller, K., Burrows, J. P., Schade, G., Solomon, S. J., Ladstatter-Weissenmayer, A., Simmonds, P., Young, D., Hopkins, J. R., Lewis, A. C., Legreid, G., Reimann, S., Hansel, A., Wisthaler, A., Blake, R. S., Ellis, A. M., Monks, P. S., and Wyche, K. P.: Intercomparison of oxygenated volatile organic compound measurements at the SAPHIR atmosphere simulation chamber, J. Geophys. Res., 113, D20307, doi:10.1029/2008JD009865, 2008.

Atkinson, R., Baulch, D. L., Cox, R. A., Crowley, J. N., Hampson, R. F., Hynes, R. G., Jenkin, M. E., Rossi, M. J., Troe, J., and IUPAC Subcommittee: Evaluated kinetic and photochemical data for atmospheric chemistry: Volume II – gas phase reactions of organic species, Atmos. Chem. Phys., 6, 3625–4055, doi:10.5194/acp-6-3625-2006, 2006.

Bohn, B., Rohrer, F., Brauers, T., and Wahner, A.: Actinometric measurements of NO$_2$ photolysis frequencies in the atmosphere simulation chamber SAPHIR, Atmos. Chem. Phys., 5, 493–503,

doi:10.5194/acp-5-493-2005, 2005.

Bottinga, Y.: Hydrogen Isotope Equilibria in System Hydrogen-Water, J. Phys. Chem., 72, 4338–4340, 1968.

Brauers, T., Bossmeyer, J., Dorn, H.-P., Schlosser, E., Tillmann, R., Wegener, R., and Wahner, A.: Investigation of the formaldehyde differential absorption cross section at high and low spectral resolution in the simulation chamber SAPHIR, Atmos. Chem. Phys., 7, 3579–3586, doi:10.5194/acp-7-3579-2007, 2007.

Brenninkmeijer, C. A. M., Janssen, C., Kaiser, J., Röckmann, T., Rhee, T. S., and Assonov, S. S.: Isotope effects in the chemistry of atmospheric trace gases, Chem. Rev., 103, 5125–5162, 2003.

Ehhalt, D. H. and Rohrer, F.: The tropospheric cycle of H$_2$: a critical review, Tellus B, 61, 500–535, 2009.

Feck, T., Grooss, J. U., and Riese, M.: Sensitivity of Arctic ozone loss to stratospheric H$_2$O, Geophys. Res. Lett., 35, L01803, doi:10.01029/02007GL031334, 2008.

Feilberg, K. L., Johnson, M. S., and Nielsen, C. J.: Relative reaction rates of HCHO, HCDO, DCDO, (HCHO)-^{13}C, and (HCHO)-^{18}O with OH, Cl, Br, and NO$_3$ radicals, J. Phys. Chem. A, 108, 7393–7398, 2004.

Feilberg, K. L., D'Anna, B., Johnson, M. S., and Nielsen, C. J.: Relative tropospheric photolysis rates of HCHO, (HCHO)-^{13}C, (HCHO)-^{18}O, and DCDO measured at the European photoreactor facility, J. Phys. Chem. A, 109, 8314–8319, 2005a.

Feilberg, K. L., Griffith, D. W. T., Johnson, M. S., and Nielsen, C. J.: The ^{13}C and D kinetic isotope effects in the reaction of CH$_4$ with Cl, Int. J. Chem. Kinet., 37, 110–118, 2005b.

Feilberg, K. L., D'Anna, B., Johnson, M. S., and Nielsen, C. J.: Relative tropospheric photolysis rates of HCHO, (HCHO)-^{13}C, (HCHO)-^{18}O, and DCDO measured at the European photoreactor facility J. Phys. Chem. A, 111, 992–992, 2007a.

Feilberg, K. L., Johnson, M. S., Bacak, A., Röckmann, T., and Nielsen, C. J.: Relative tropospheric photolysis rates of HCHO and HCDO measured at the European photoreactor facility, J. Phys. Chem. A, 111, 9034–9046, 2007b.

Gerst, S. and Quay, P.: The deuterium content of atmospheric molecular hydrogen: Method and initial measurements, J. Geophys. Res., 105, 26433–26445, 2000.

Gerst, S. and Quay, P.: Deuterium component of the global molecular hydrogen cycle, J. Geophys. Res., 106, 5021–5031, 2001.

Gierzak, T., Talukdar, R. K., Herndon, S. C., Vaghjiani, G. L., and Ravishankara, A. R.: Rate coefficients for reactions of hydroxyl radicals with methane and deuterated methanes, J. Phys. Chem., 101, 3125–3134, 1997.

McQuigg, R. D. and Calvert, J. G.: The Photodecomposition of CH$_2$O, CD$_2$O, CHDO, and CH$_2$O-CD$_2$O Mixtures at Xenon Flash Lamp Intensities, J. Am. Chem. Soc., 91, 1590–1599, 1969.

Nilsson, E. J. K., Johnson, M. S., Taketani, F., Matsumi, Y., Hurley, M. D., and Wallington, T. J.: Atmospheric deuterium fractionation: HCHO and HCDO yields in the CH$_2$DO + O$_2$ reaction, Atmos. Chem. Phys., 7, 5873–5881, doi:10.5194/acp-7-5873-2007, 2007.

Nilsson, E. J. K., Andersen, V. F., Skov, H., and Johnson, M. S.: Pressure dependence of the deuterium isotope effect in the photolysis of formaldehyde by ultraviolet light, Atmos. Chem. Phys., 10, 3455–3462, doi:10.5194/acp-10-3455-2010, 2010.

Novelli, P. C., Lang, P. M., Masarie, K. A., Hurst, D. F., Myers, R., and Elkins, J. W.: Molecular hydrogen in the troposphere: Global distribution and budget, J. Geophys. Res., 104, 30427–30444, 1999.

Pieterse, G., Krol, M. C., and Röckmann, T.: A consistent molecular hydrogen isotope chemistry scheme based on an independent bond approximation, Atmos. Chem. Phys., 9, 8503–8529, doi:10.5194/acp-9-8503-2009, 2009.

Price, H., Jaegle, L., Rice, A., Quay, P., Novelli, P. C., and Gammon, R.: Global budget of molecular hydrogen and its deuterium content: Constraints from ground station, cruise, and aircraft observations, J. Geophys. Res., 112, D22108, doi:22110.21029/22006JD008152, 2007.

Rahn, T., Eiler, J. M., Kitchen, N., Fessenden, J. E., and Randerson, J. T.: Concentration and dD of molecular hydrogen in boreal forests: Ecosystem-scale systematics of atmospheric H$_2$, Geophys. Res. Lett., 29, 1888, doi:10.1029/2002GL015118, 2002a.

Rahn, T., Kitchen, N., and Eiler, J. M.: D/H ratios of atmospheric H$_2$ in urban air: Results using new methods for analysis of nanomolar H$_2$ samples, Geochim. Cosmochim. Acta, 66, 2475–2481, 2002b.

Rahn, T., Eiler, J. M., Boering, K. A., Wennberg, P. O., McCarthy, M. C., Tyler, S., Schauffler, S., Donnelly, S., and Atlas, E.: Extreme deuterium enrichment in stratospheric hydrogen and the global atmospheric budget of H$_2$, Nature, 424, 918–921, 2003.

Rhee, T. S., Mak, J. E., Brenninkmeijer, C. A. M., and Röckmann, T.: Continuous-flow isotope analysis of the D/H ratio in atmospheric hydrogen, Rap. Commun. Mass Spectrom., 18, 299–306, 2004.

Rhee, T. S., Brenninkmeijer, C. A. M., and Rckmann, T.: The overwhelming role of soils in the global atmospheric hydrogen cycle, Atmos. Chem. Phys., 6, 1611–1625, doi:10.5194/acp-6-1611-2006, 2006.

Rhee, T. S., Brenninkmeijer, C. A. M., Brass, M., and Brühl, C.: Isotopic composition of H$_2$ from CH$_4$ oxidation in the stratosphere and the troposphere, J. Geophys. Res., 111, D23303, doi:23310.21029/22005JD006760, 2006.

Rhee, T. S., Brenninkmeijer, C. A. M., and Rckmann, T.: Hydrogen isotope fractionation in the photolysis of formaldehyde, Atmos. Chem. Phys., 8, 1353–1366, doi:10.5194/acp-8-1353-2008, 2008.

Rice, A. L. and Quay, P. D.: Isotopic analysis of atmospheric formaldehyde by gas chromatography isotope ratio mass spectrometry, Anal. Chem., 78, 6320–6326, 2006.

Röckmann, T., Rhee, T. S., and Engel, A.: Heavy hydrogen in the stratosphere, Atmos. Chem. Phys., 3, 2015–2023, doi:10.5194/acp-3-2015-2003, 2003.

Röckmann, T., Gómez Álvarez, C. X., Walter, S., Veen, C. v., Wollny, A. G., Gunthe, S. S., Helas, G., Pöschl, U., Keppler, F., Greule, M., and Brand, W. A.: The isotopic composition of H$_2$ from wood burning – dependency on combustion efficiency, moisture content and δD of local precipitation, J. Geophys. Res., doi:10.1029/2009JD013188, in press, 2010.

Rohrer, F., Bohn, B., Brauers, T., Brning, D., Johnen, F.-J., Wahner, A., and Kleffmann, J.: Characterisation of the photolytic HONO-source in the atmosphere simulation chamber SAPHIR, Atmos. Chem. Phys., 5, 2189–2201, doi:10.5194/acp-5-2189-2005, 2005.

Sander, S. P., Friedl, R. R., Golden, D. M., Kurylo, M. J., Moortgat, G. K., Keller-Rudek, H., Wine, P. H., Ravishankara, A. R., Kolb, C. E., Molina, M. J., Finlayson-Pitts, B. J., Huie, R. E., and

Orkin, V. L.: Chemical Kinetics and Photochemical Data for Use in Atmospheric Studies, Evaluation Number 15, JPL Publication 06-2, Jet Propulsion Laboratory, Pasadena, 2006.

Schultz, M. G., Diehl, T., Brasseur, G. P., and Zittel, W.: Air pollution and climate-forcing impacts of a global hydrogen economy, Science, 302, 624–627, 2003.

Steele, L. P., Langenfelds, R. L., Lucarelli, M. P., Fraser, P. J., Cooper, L. N., Spenser, D. A., Chea, S., and Broadhurst, K.: Atmospheric methane, carbon dioxide, carbon monoxide, hydrogen, and nitrous oxide from Cape Grim air samples analysed by gas chromatography, in: Baseline Atmospheric Program Australia, 1994–1995, edited by: Francey, R. J., Dick, A. L., and Derek, N., 107–110, 1996.

Tromp, T. K., Shia, R.-L., Allen, M., Eiler, J. M., and Yung, Y. L.: Potential Environmental Impact of a Hydrogen Economy on the Stratosphere, Science, 300, 1740–1742, 2003.

Vollmer, M. K., Walter, S., Bond, S. W., Soltic, P., and Röckmann, T.: Molecular hydrogen (H₂) emissions and their isotopic signatures (H/D) from a motor vehicle: implications on atmospheric H₂, Atmos. Chem. Phys. Discuss., 10, 3021–3051, doi:10.5194/acpd-10-3021-2010, 2010.

Warwick, N. J., Bekki, S., Nisbet, E. G., and Pyle, J. A.: Impact of a hydrogen economy on the stratosphere and troposphere studied in a 2-D model, Geophys. Res. Lett., 31, L05107, doi:05110.01029/02003GL019224, 2004.

Wisthaler, A., Apel, E. C., Bossmeyer, J., Hansel, A., Junkermann, W., Koppmann, R., Meier, R., Mller, K., Solomon, S. J., Steinbrecher, R., Tillmann, R., and Brauers, T.: Technical Note: Intercomparison of formaldehyde measurements at the atmosphere simulation chamber SAPHIR, Atmos. Chem. Phys., 8, 2189–2200, doi:10.5194/acp-8-2189-2008, 2008.